

GRAB: A Systematic Real-World Grasping Benchmark for Robotic Food Waste Sorting

Moniesha Thilakarathna*, Xing Wang*, Min Wang, David Hinwood, Shuangzhe Liu, Damith Herath

Moniesha Thilakarathna, Dr.Xing Wang, Dr.Min Wang, Dr.David Hinwood, Assoc Prof. Shuangzhe Liu, Prof. Damith Herath

Address: Faculty of Science and Technology, University of Canberra, 11 Kirinari St, Bruce ACT 2617, Australia

Email Address: Moniesha.Thilakarathna@canberra.edu.au, Xing.Wang@canberra.edu.au

Keywords: *Robotic Food Waste Sorting, Robotic Grasping, Grasp benchmarking*

Food waste management is critical for sustainability, yet inorganic contaminants hinder recycling potential. Robotic automation presents a compelling approach to this challenge by accelerating the sorting process through automated contaminant removal. Still, the diverse and unpredictable nature of contaminants creates major challenges for robotic grasping. Benchmarking frameworks are critical for evaluating challenges from various perspectives. However, existing protocols rely on limited simulation datasets, prioritise simple metrics such as success rate, and overlook key object and environment-related pre-grasp conditions. This paper introduces GRAB, a comprehensive Grasping Real-World Article Benchmarking framework that addresses this gap by integrating diverse deformable objects, advanced grasp-pose-estimation vision, and, importantly, pre-grasp conditions, establishing a set of critical graspability metrics. It systematically compares industrial grasping modalities through an in-depth experimental evaluation involving 1,750 food contaminant grasp attempts across four high-fidelity scenes. This large-scale evaluation provides an extensive assessment of grasp performance for food waste sorting, offering a level of depth that has rarely been explored in previous studies. The results reveal distinct gripper strengths and limitations, with object quality emerging as the dominant performance factor in cluttered environments, while vision quality and clutter levels play moderate roles. These findings highlight essential design considerations and reinforce the necessity of developing multimodal gripper technologies capable of robust cross-category performance for effective robotic food waste sorting.

1 Introduction

The growing global population is compounding municipal solid waste (MSW) management challenges. Organic waste comprising 19% of MSW and primarily from food sources [1] amounts to 4.7 million tonnes in Australia. Recycling food waste is vital for a sustainable economy, yet the process is hindered by inorganic contaminants (Figure 1). While uncontaminated food waste can be repurposed for low-emission applications like protein farming [2], segregation remains predominantly manual due to waste stream heterogeneity. Robotic deployment in food waste sorting faces unique recognition and grasping challenges arising from clutteriness [3, 4], rigid-deformable object coexistence [5], and general unstructured conditions. The efficiency of robotic waste sorting can be enhanced through improvements in computer vision-based detection accuracy or by augmenting the grasping performance of end-effectors. While significant research has focused on advancing visual intelligence, a growing need exists to enhance the physical intelligence of grasping systems, where selecting the correct grasping mode is pivotal for addressing the domain’s inherent complexities.

Benchmarking provides a scientifically rigorous methodology for validating performance and determining optimal grasping strategies in multi-object scenarios. Industrial evaluations primarily rely on operational speed (mean picks per hour), and reliability metrics mostly grasp success rates [6] from established datasets [7]. However, the fixed taxonomies of these standardized datasets limit their applicability to novel object categories in dynamic applications such as food waste sorting. Contemporary research underscores that grasp performance is highly dependent on application-specific conditions [8], [9], demanding evaluation frameworks that extend beyond success rates. This recognition has spurred the development of advanced protocols incorporating multi-object metrics [10] and gripper-specific factors [11]. However, comprehensive evaluations must also account for environmental and object-specific pre-grasp conditions [12].

To our best knowledge, current grasp performance evaluation lacks a systematic pipeline for assessing how object, vision, and environmental pre-grasp conditions collectively shape grasping performance, and a unified metric for comparing gripper performance in specific applications remains absent. This paper introduces GRAB, a systematic Grasping Real-World Article Benchmarking framework designed to evaluate standard grasping modes on diverse real-world objects under application-specific pre-grasp conditions, using food waste sorting as the primary use case.



Figure 1: Industrial-scale variation of inorganic contaminants inside food waste

Preliminary results introducing a subset of the automated robotic grasp benchmarking pipeline and a comparative evaluation of three grippers under varied conditions were first reported in [13]. The work presented here represents the complete, comprehensive realisation of benchmarking research, including new scientific findings through expanded hardware, metrics, and validation. It takes an important step toward investigating the effects of vision score, object quality, and environmental-complexity-related metrics on evaluation performance. We evaluate their combined influence using three distinct performance measures, which strengthens the generalisability of the proposed benchmarking framework for use beyond food-waste sorting and across diverse cluttered environments. To summarise, our contributions are as follows:

- We introduce a novel benchmarking framework to evaluate the performance of grasping modalities while extracting inorganic contaminants from food waste, incorporating object, vision, and environment-related pre-grasp metrics tested through a real-world grasp benchmarking pipeline.
- We present a systematic and in-depth comparative performance evaluation of three uni-modal grippers across four high-fidelity environmental scenes to identify how different grasping modes respond to diverse object categories in cluttered food waste scenes, providing valuable insights into the potential for cross-category grasping.
- We provide a comprehensive analysis of how pre-grasp conditions affect overall grasp performance and their significant relationships.
- We present a comparative evaluation of grasp failure modes and the impact of pre-grasp conditions on failure cases.

2 Related Works

2.1 Robotic Waste Sorting

The efficacy of robotic waste sorting has been substantially advanced through developments in artificial intelligence (AI) and automation, as demonstrated by industry leaders like AMP Robotics achieving up to 99% sorting accuracy for recyclables using deep learning (DL) [14]. This progress is further evidenced by recent innovations: Adetunji et al. developed a vacuum system employing convolutional neural networks to detect plastic bags [15], Maxence et al. created a 4-DoF (4D) parallel robot with a suction gripper for recyclables [16], and Xinxing et al. implemented a DL based mobile robot for construction waste [17]. While robotic sorting typically targets recyclables like glass, paper, plastic, and metals for resource recovery, a significant yet under-explored application is food waste recycling, where automation could enhance sorting efficiency and reduce worker health risks.

2.2 Grasp Vision in Waste Sorting

Vision intelligence remains crucial for robotic waste sorting, where machine learning algorithms like Faster R-CNN, Mask R-CNN, and YOLO enable waste identification [18, 19]. However, they lack the spatial detail for successful grasping, necessitating algorithms that accurately identify the ideal Grasp Pose (GP) with position and orientation. Early GP Detection (GPD) methods estimated 3D or 4D poses as rectangles [20],

though this fixed-angle approach limited clutter adaptability [21]. Contemporary 6D-GPD addresses this by estimating full 6D configurations for enhanced flexibility [22]. Conventional 6D-GPD models requiring CAD data are impractical for waste sorting, prompting a shift to data-driven approaches like generating GPs from voxelized point clouds [23] and PointNetGPD’s fine-grained quality prediction [24]. A persistent challenge is robust estimation from noisy point clouds with limited datasets. GraspNet addresses this via synthetic-real data integration [25], a framework later advanced by GSNet’s [26] geometric structure encoder for improved reasoning in cluttered scenes. This lineage culminates in the AnyGrasp system, which builds upon GSNet to handle significant depth-noise and incorporate stability awareness [27]. Beyond parallel jaws, suction-based grasping has received significant attention. Dex-Net 3.0 generates suction poses from depth images but declines in cluttered bins [28]. Another method improves orientation accessibility but requires complex pre-manipulation [29]. In contrast, SuctionNet predicts stable poses directly from RGB-D images using end-to-end deep learning, eliminating heuristics for superior adaptability in waste environments [30].

2.3 Grippers for Waste Grasping

A significant challenge in AI-driven robotic waste sorting involves developing grasping systems for extreme object diversity in highly cluttered environments [31]. This demands not only advanced perception but also enhanced physical intelligence. Current industrial waste sorting systems primarily utilize two gripper types: suction grippers for lightweight objects with relatively flat surfaces [14], and rigid grippers for standard recyclables and heavier debris like construction waste [32, 33]. While effective within their niches, these traditional designs lack full waste spectrum versatility compared to emerging soft grippers offering adaptive compliance [34]. Recognizing that no single gripper is universally optimal, the research field is shifting toward multi-modal designs combining several grasping mechanisms [31], exemplified by Rasoul et al.’s vision-guided, tri-modal gripper achieving 96% success in controlled recyclable sorting [35].

2.4 Grasp Benchmarking

Grasp performance varies with the application or application-specific conditions [6], necessitating tailored benchmarking approaches [8]. Such research requires systematic methodologies involving representative object selection, candidate gripper selection, and comprehensive evaluation systems that extend beyond basic success rates to include application-specific metrics and quantitative scoring mechanisms [9]. Moreover, experimental design substantially influences grasping outcomes, with factors including robot arm selection and task complexity ranging from single-object to multi-object picking [6]. Recent work has expanded benchmarking to multi-object scenarios, employing metrics like picking accuracy, overall success rate, availability rate, and cost per unit [10], while others have addressed gripper-specific factors through additional metrics measuring grasp strength, finger strength, and repeatability, alongside common measures like cycle time [11]. Similarly, environmental and pre-grasp conditions also critically impact performance [8].

Fundamentally, successful grasping involves more than simply picking and placing an object. It requires understanding object properties, whether soft, rigid, or delicate, identifying the correct object pose, and assessing environmental factors like occlusion and isolation as humans do. Effective grasping depends on evaluating these pre-grasp conditions to determine appropriate grasping strategies. Current research lacks an integrated real-world benchmarking framework that simultaneously evaluates comprehensive grasp performance metrics and the impact of pre-grasp conditions, including object state, vision quality, and surrounding environmental factors, on overall grasp performance.

3 Methodology

This section details the proposed benchmarking methodology, divided into two primary components: the robotic grasping pipeline and the evaluation framework. First, we describe the system architecture, comprising the grasp pose estimation algorithm, physical grasping modules, and path planning strategies. Second, we define ‘graspability’ in the context of pre-grasp environmental conditions and outline the quantitative metrics used to assess performance.

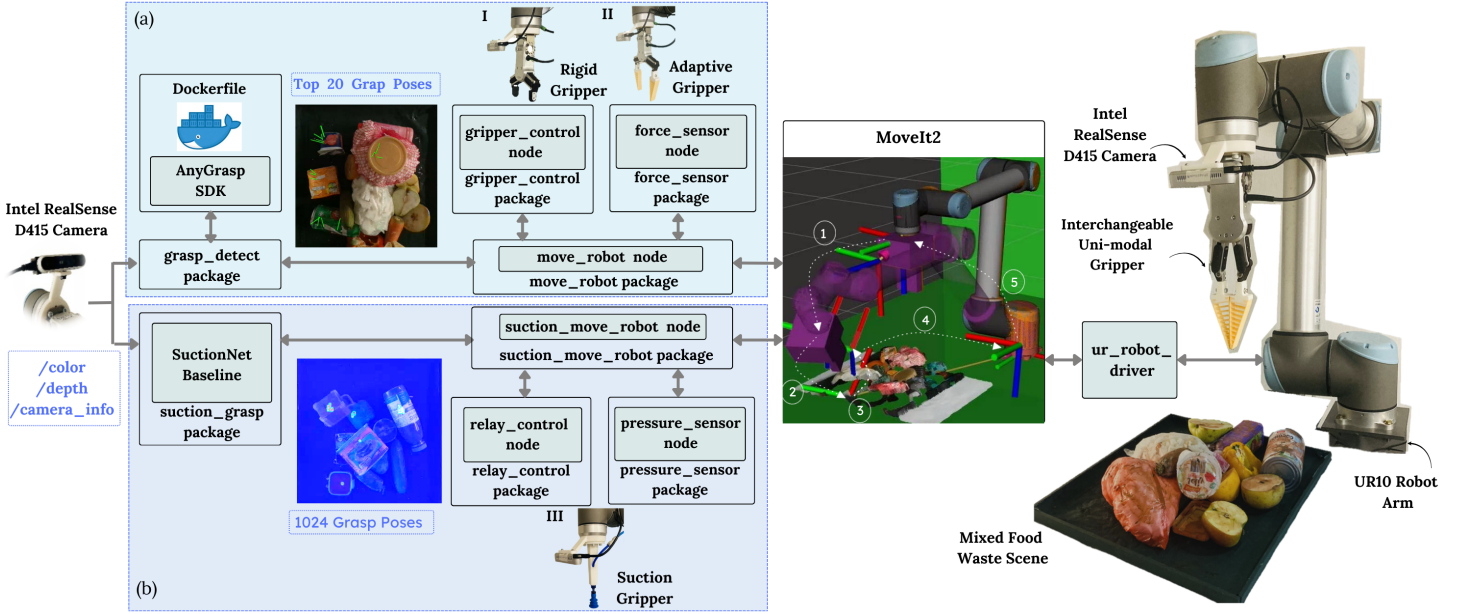


Figure 2: Conceptualization of the real-world robotic grasping pipeline using the ROS 2 control stack: (a) for the rigid force-controlled parallel gripper (RG2) and adaptive Fin-Ray gripper, and (b) for the suction gripper. MoveIt2 block highlights a snapshot of the MoveIt 2 path planning GUI, displaying the home pose (arm), pre-grasp pose (purple arm) after trajectory planning, and the grasp pose in the waste scene, post-grasp pose and drop pose.

3.1 Grasp Benchmarking Pipeline

The integrated robotic grasping pipeline is built upon three core components: a 6D-GPD system for advanced visual perception, three grasping modes including three interchangeable robotic grippers with integrated sensors for high-quality grasping and a 6 DoF industrial robotic arm for collision-free path planning, as shown in Figure 2. The system comprises an Intel RealSense D415 camera for 6D-GPD, a 6 DoF UR10 robotic arm for path planning and manipulation, and a Lenovo Legion RTX 4070 laptop operating on Ubuntu 22.04 with the ROS 2 Humble distribution for processing and control, in addition to three industrial grippers. The complete pipeline is administered by ROS 2 packages, which provide sensor data processing, grasp pose generation and evaluation, grasp selection, path planning and trajectory execution, and grasp execution. To accommodate the three distinct gripper modalities, the system employs two specialized 6D-GPD models. The AnyGrasp model [27] is utilized to export top-ranking grasping poses for both the parallel grippers, leveraging its robustness to sensor noise and strong generalization to novel objects. For the suction gripper, the system implements SuctionNet [30], selected for its end-to-end ability to predict stable suction poses directly from RGB-D data. Both models were adapted and integrated into the ROS 2 control stack. The UR10 robotic arm performs collision-free trajectories with MoveIt 2. Actuation of the end-effectors is handled through multiple interfaces: the RG2 gripper is controlled directly via the robot’s controller, whereas the suction gripper is operated by a pneumatic system driven by an Arduino microcontroller integrated with ROS 2.

3.1.1 Grasp Pose Detection Module

The vision system implementation began with eye-in-hand camera calibration. Intrinsic parameters were calibrated using a MATLAB toolbox, achieving a mean re-projection error of 0.17 pixels. The transformation from pixel coordinates (u, v) to camera coordinates (X_c, Y_c, Z_c) is calculated using the depth value Z_c and intrinsic parameters:

$$\begin{pmatrix} X_c \\ Y_c \\ Z_c \end{pmatrix} = \begin{pmatrix} \frac{1}{f_x} & 0 & -\frac{c_x}{f_x} \\ 0 & \frac{1}{f_y} & -\frac{c_y}{f_y} \\ 0 & 0 & 1 \end{pmatrix} \begin{pmatrix} u \\ v \\ Z_c \end{pmatrix} \quad \text{Equation (1)}$$

Where c_x, c_y : Principal point (optical center) in pixels, f_x, f_y : Focal lengths in pixels, Z_c : Depth along optical axis. World coordinates (X_w, Y_w, Z_w) are then obtained through the transformation:

$$(X_w, Y_w, Z_w, 1)^T = \mathbf{T}_{\text{world}}^{\text{cam}}(X_c, Y_c, Z_c, 1)^T \quad \text{Equation (2)}$$

where $\mathbf{T}_{\text{world}}^{\text{cam}}$ combines the eye-in-hand calibration matrix and the UR10’s forward kinematics:

$$\mathbf{T}_{\text{world}}^{\text{cam}} = \mathbf{T}_{\text{base}}^{\text{cam}} = \mathbf{T}_{\text{base}}^1 \mathbf{T}_1^2 \mathbf{T}_2^3 \mathbf{T}_3^4 \mathbf{T}_4^5 \mathbf{T}_5^6 \mathbf{T}_{\text{ee}}^{\text{ee}} \mathbf{T}_{\text{ee}}^{\text{cam}} \quad \text{Equation (3)}$$

The homogeneous transformation matrix from the camera to the end effector, $\mathbf{T}_{\text{ee}}^{\text{cam}}$, is derived using the respective function in MATLAB’s moving camera calibration strategy. This overall calibration process enables the robot to correctly interpret visual information from the camera in its own coordinate system. The selected 6D-GPD models output poses in their native formats, which require conversion to standardized homogeneous transformation matrices for integration with the MoveIt2 motion planning framework. AnyGrasp represents grasp poses as:

$$G = [R \quad t \quad w] \quad \text{Equation (4)}$$

where, $R \in \mathbb{R}^{3 \times 3}$ denotes the gripper orientation, $t \in \mathbb{R}^{3 \times 1}$ denotes the center of grasp, and $w \in \mathbb{R}$ the minimum gripper width that is suitable for grasping the target object. Each candidate’s grasp receives a quality score combining geometric assessment and stability evaluation. The base grasp score from GSNet analyzes scene-level geometry features, while the stable score measures the normalized perpendicular distance from the gripper plane to the object’s center of gravity. The final score is computed as: final grasp score = original grasp score \times (1 – stable score) with scores for collision-prone grasps set directly to zero. The system then re-parameterizes poses into 7-DoF configurations and ranks them by this final score, ensuring that selected grasps balance both geometric feasibility and stability.

SuctionNet [30] analyzes RGB-D images by generating two heatmaps: a seal score heatmap and a center score heatmap. The ultimate suction score map is derived by multiplying these two heatmaps. Due to the high density of projected values, SuctionNet identifies the highest-scoring suction candidate within each grid, ranks these candidates, and outputs the pixel coordinates of the top 1024 suction points. These pixels are then projected into three-dimensional space to determine their spatial locations. The suction directions are established by computing surface normals at the corresponding points. Mathematically, the suction representation is defined as:

$$S = [p \quad u] \quad \text{Equation (5)}$$

where p represents the suction point, the center of contact, and u is the unit vector indicating the direction from the suction point outward from the object’s surface. We convert grasp poses from both models into the robot’s coordinate system by first aligning the gripper’s z-axis outward, then applying coordinate transformations. The resulting rotation is converted to quaternions, producing standardized poses (3D translation + quaternion) accompanied by quality scores. These transformed poses provide MoveIt2 with the necessary information to plan and execute collision-free motion trajectories to the target grasp locations.

3.1.2 Grasping Modes

Three gripper modalities employed are: (a) the rigid force-controlled parallel gripper (RG2), (b) the soft adaptive Fin-Ray gripper, and (c) the suction gripper (Figure 3), which are designed to accommodate various object features and improve grabbing efficacy. In RG2, the parallel jaw mechanism ensures a solid and steady grip, rendering it especially appropriate for manipulating items with well-defined geometric characteristics. We set a constant force output of 40 N by controlling the driving motor’s current output. The adaptive two-finger parallel gripper is created by modifying the RG2 gripper’s fingers with a baseline Fin-Ray soft finger [36]. This change enables the gripper to passively adapt to an object’s contours, enhancing its capacity to grab irregular items. The modality, pneumatic suction, produces optimal adhesion force at a maximum vacuum pressure of –80 kPa, where the suction cup adheres to the target surface by creating a pressure differential between the reduced pressure inside the suction cup and the ambient atmospheric pressure, thus generating a normal force that holds the object in place.

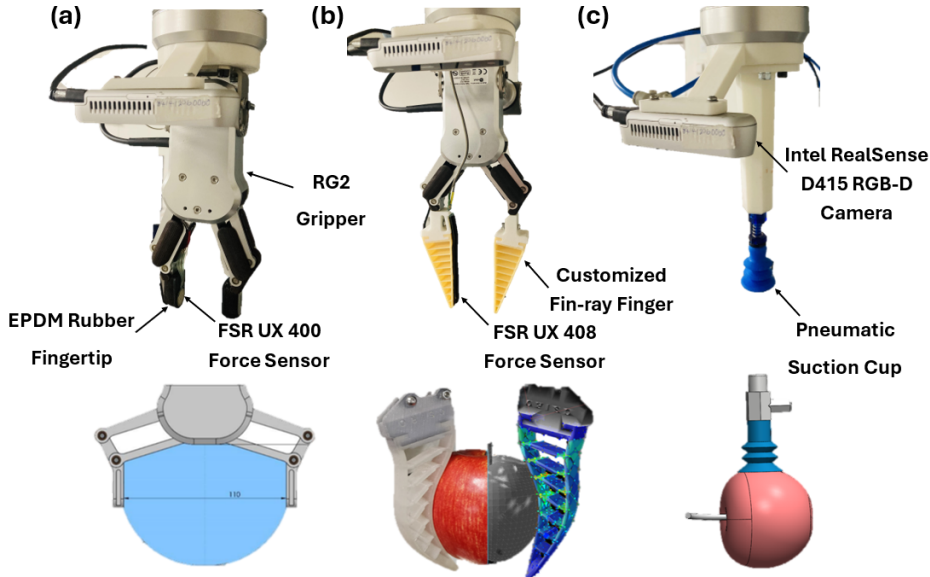


Figure 3: Three distinct grasping modes (a) Rigid force-controlled two-finger parallel gripper (RG2) with FSR UX 400 force sensor (b) Soft adaptive two-finger Fin-Ray gripper with FSR UX 408 force sensor (c) Suction Gripper

3.1.3 Path Planning and Grasp Activation

The grasping process adheres to a systematic series of five essential poses: Home Pose, Pre-Grasp Pose, Grasp Pose, Post-Grasp Pose, and Drop Pose (see Figure 2 and the attached video for further details). Grasp candidates are initially predicted using 6D-GPD networks, from which the top eight grasp poses are chosen, and each is characterized by a location and an orientation (in quaternion representation). Among the highest-ranked grasp poses, the ultimate execution Grasp Pose is chosen based on two post-processing criteria: (1) the pose must be collision-free with the workbench, verified using MoveIt Flexible Collision Library, and (2) its approach vector must create an angle of no less than 30 degrees with the workbench plane to reduce occlusions and guarantee collision-free execution. As mentioned in section 3.2.1, grasp poses, initially referred to the camera frame, are then translated into the gripper frame with the rigid transformation \mathbf{T}_{ee}^{cam} . The Pre-Grasp pose is calculated by offsetting backwards along the approach vector, facilitating seamless transitions and avoiding collisions. The integration of both pre-grasp and post-grasp positions is essential for preventing unintended collisions with adjacent objects during execution.

MoveIt2 serves as the principal framework for motion planning, utilizing the Rapidly-exploring Random Tree (RRT) - state-of-the-art route planning algorithm from the Open Motion Planning Library (OMPL) to produce collision-free trajectories. To improve trajectory accuracy, cartesian path planning utilizing linear interpolation is employed, ensuring smooth and predictable end-effector movement. This is further refined by enforcing velocity and acceleration constraints to guarantee kinematically feasible movements that prevent sudden jerks and protect grasp integrity.

3.2 Graspability Conditions & Evaluation Metrics

In our framework, we define an object’s ability to be grasped (Graspability) in a cluttered environment primarily based on three pre-grasp conditions: the quality of the object itself, the quality of the vision system, and the influence of clutter. Together, these conditions determine the overall status of the object before grasping. We identify these as graspability parameters, and they are the key drivers that influence grasp performance. Hence, it is important to evaluate the impact of these parameters to benchmark the performance of the grasping modes in a complex environment like food waste sorting. Along with, we evaluate three grasp performance parameters: grasp success, grasp stability, and grasp efficiency for each grasping attempt.

3.2.1 Graspability Parameters

Graspability parameters directly affect the gripper’s ability to successfully grasp an object. To ensure fair evaluation of each grasping mode, the object being grasped must itself demonstrate a reasonable ability

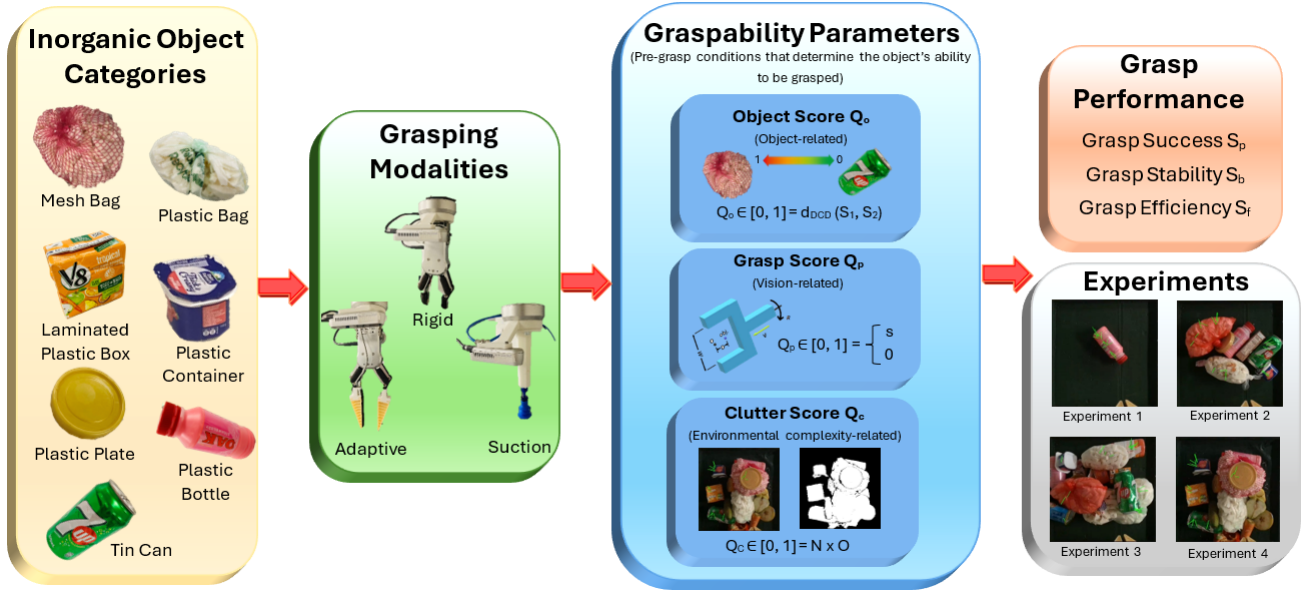


Figure 4: Grasp benchmarking framework showing the integration of grasping modalities, graspability parameters that characterize pre-grasp conditions, and performance assessment using high-fidelity experiments.

to be grasped by the gripper. In our framework, each grasp cycle is quantitatively analysed through three graspability parameters: object score, grasp score, and clutter score.

Object Score (Q_o):

Our primary object dataset originates from industrial field research (Figure 1), which identified seven predominant categories of inorganic food waste contaminants: Plastic Bags, Plastic Containers, Plastic Plates, Plastic Bottles, Laminated Paper Boxes (LPB), Mesh Bags, and Tin Cans. These categories collectively represent approximately 88% of inorganic waste materials, establishing the core testbed for our experimental investigations. Three representative items were collected from each category, resulting in a total of 21 distinct objects for experimentation. All selected objects weighed less than 100 g, which is below the allowable payload of the grippers, and had a cubic volume within $20 \times 10 \times 10 \text{ cm}^3$, making them suitable for the gripper widths and the negative pressure of the suction gripper. Unlike published datasets, this object dataset includes both rigid and deformable objects, covering a significant span of geometric variation. Because the weight and size were controlled to satisfy the gripper constraints, object deformation or shape variation emerged as the primary factor influencing graspability. Therefore, deformation was parameterized as the object-related graspability condition, defined as the Object Score Q_o .

To measure object deformation, 3D point clouds are captured in the object's initial state and again while it is gripped under a 40 N compression force. The difference between these two states is calculated using the Density-Aware Chamfer Distance (DCD) metric [37]. DCD offers a significant advantage over standard metrics such as Chamfer Distance or Earth Mover's Distance because it is robust against uneven

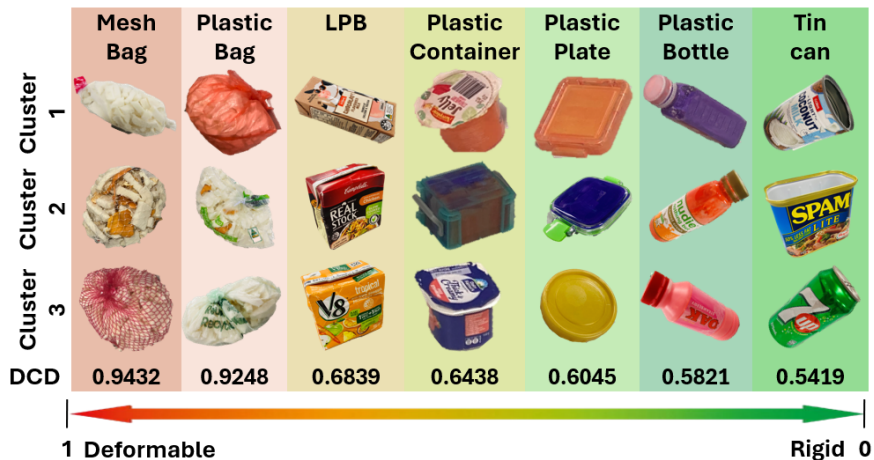


Figure 5: Object dataset with their corresponding average DCD values

point density and the presence of outlier points [38]. This robustness allows for consistent and reliable measurement even with partial occlusions, which is why DCD is well-suited for deformation analysis using incomplete point clouds.

The DCD algorithm is defined as:

$$d_{\text{DCD}}(S_1, S_2) = \frac{1}{2} \left(\frac{1}{|S_1|} \sum_{x \in S_1} \left(1 - \frac{1}{\hat{n}_y} e^{-\alpha \|x - \hat{y}\|_2} \right) + \frac{1}{|S_2|} \sum_{y \in S_2} \left(1 - \frac{1}{\hat{n}_x} e^{-\alpha \|y - \hat{x}\|_2} \right) \right) \quad \text{Equation (6)}$$

Here, $\hat{y} = \min_{y \in S_2} \|x - y\|_2$ and $\hat{x} = \min_{x \in S_1} \|y - x\|_2$. The metric computes the average distance between each point in one point cloud (S_1) and its nearest neighbor in the other (S_2). To ensure that distances are comparable and bounded, they are normalized into the range $[0, 1]$. This is achieved by approximating the exponential term using a first-order Taylor expansion, $e^z \approx 1 - \|z\|_2$ which guarantees that small distances are mapped close to 0 while larger distances saturate towards 1. The scalar parameter α controls the sensitivity of this mapping and tunes how quickly the metric penalizes deformation.

A custom experimental platform was developed to capture 3D point clouds of the objects before and after being gripped under a 40 N compression force (Figure 6). The setup consisted of an UR10 robot arm, an RG2 gripper with custom-made compression pads, and a customized 3D scanning platform integrated with an Intel RealSense D415 RGB-D camera. The objects were compressed along both the x- and y-planes, and the averaged DCD values were calculated. For acquiring the 3D point clouds, the RecFusion 3D reconstruction software was used. To evaluate these point clouds, the grasped objects needed to be segmented from the 3D scene and isolated from both the grippers and the background. To facilitate this process, the scene was configured to have high contrast: the test objects were placed on a plain background, and the test grippers were printed in the same colour. Background removal and filtering were performed using both RecFusion and MeshLab software.

To accurately measure deformation and correct for small in-hand orientation shifts, the pre- and post-grasp point clouds were aligned during post-processing. Since different parts of the object become visible before and after grasping, the two point clouds exhibit varying feature sets, making alignment essential.

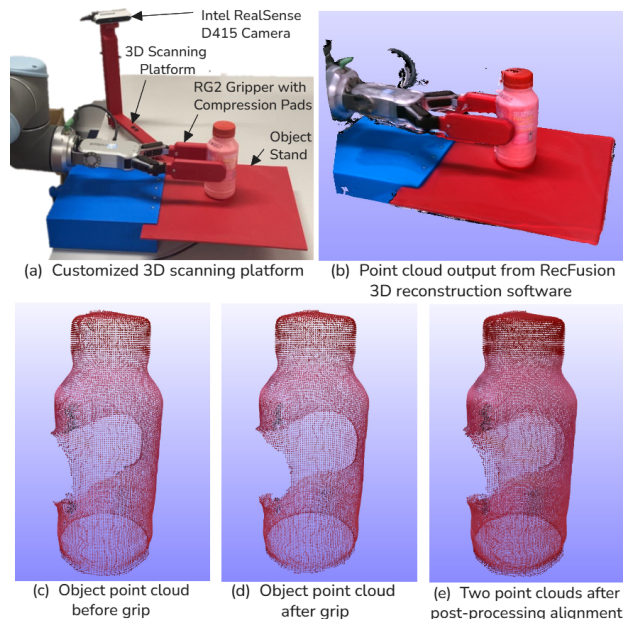


Figure 6: Overview of 3D scanning and point-cloud processing workflow for DCD computation (a) Customized 3D scanning and compression platform, (b) RecFusion 3D reconstruction, (c) point cloud of the undeformed object before gripping, (d) point cloud of the deformed object under compression, and (e) aligned point clouds illustrating geometric differences due to deformation.

The alignment was performed in two stages: first, the principal axes of the point clouds were aligned using MeshLab to provide an initial coarse registration; then, the Iterative Closest Point (ICP)[39] algorithm was applied to refine the alignment and minimize the residual distance between the two point clouds.

Grasp Score (Q_p) :

The grasp score quantifies the vision system’s effectiveness in generating feasible grasp poses within cluttered scenes. Specifically, it is defined as the final score from AnyGrasp [27] for parallel-jaw grasping and the suction score from SuctionNet [30] for suction-based grasping. These models were selected for their state-of-the-art performance and demonstrated robustness in cluttered environments: AnyGrasp provides strong zero-shot generalization to novel objects, while SuctionNet enables end-to-end pose prediction without complex heuristics. We intentionally use these scores directly without modification. This approach establishes the vision system as a fixed, high-performance benchmark, thereby isolating the physical grasping capability of the end-effectors as the primary variable under investigation.

As outlined in section 3.1.1, for each grasp attempt, the top-ranked grasp poses proposed by the vision system are further filtered through two post-processing criteria. If a grasp pose meets these execution conditions, the score assigned by the vision system is recorded as s . Conversely, if no valid grasp pose is generated for an object, the score is set to 0. Grasp execution and subsequent performance evaluation are only conducted when valid grasp poses are successfully generated. This relationship is formally expressed as:

$$Q_p \in [0, 1] = \begin{cases} s, & \text{final grasp score provided by the vision} \\ & \text{system satisfying execution conditions} \\ 0, & \text{if no valid grasp pose is generated} \end{cases} \quad \text{Equation (7)}$$

Clutter Score (Q_c) :

Most existing grasp benchmarking systems face challenges when dealing with cluttered and irregular scenes [10], particularly when comparing grasping modes for a given task. In our framework, we introduce a clutter score to quantify the clutteriness of a scene with multiple objects. The clutter score $Q_c \in [0, 1]$ reflects how the complexity of clutter influences the ability to grasp an object. It is defined by two parameters: the proportion of the workspace occupied by objects (occupancy) and the total number of objects present in the scene at a given time. Each grasping run begins with a larger number of objects in a scene, resulting in higher occupancy. As objects are grasped and removed during successive cycles, both the number of objects and the occupancy gradually decrease. It is computed only for trials where more than one object exists in the scene. In single-object trials, where no additional objects are present in the scene, clutter impact is not applicable.

$$Q_c = \begin{cases} N \times O, & N_{\text{initial scene}} > 1 \\ 0, & N_{\text{initial scene}} = 1 \quad (\text{no clutter}) \end{cases} \quad \text{Equation (8)}$$

$$N = \frac{N_{\text{before trial}}}{N_{\text{initial scene}}}, \quad O = \frac{O_{\text{before trial}}}{O_{\text{initial scene}}} \quad \text{Equation (9)}$$

where:

O : Occupancy ratio for the grasp trial,

N : Object ratio for the grasp trial.

Occupancy was calculated through a sequence of filtering steps applied to the RGB-D data. The workspace mask was first binarised to separate the valid workspace from the background. Contours were then extracted to retain only the outermost boundary. The contour was compressed by removing redundant points and retaining only the essential vertices [40]. The largest contour was selected as the effective workspace, acting as a contour-based spatial filter, and further refined by horizontal and vertical trimming to eliminate boundary artifacts. In addition, a depth filter was applied to the depth image, restricting

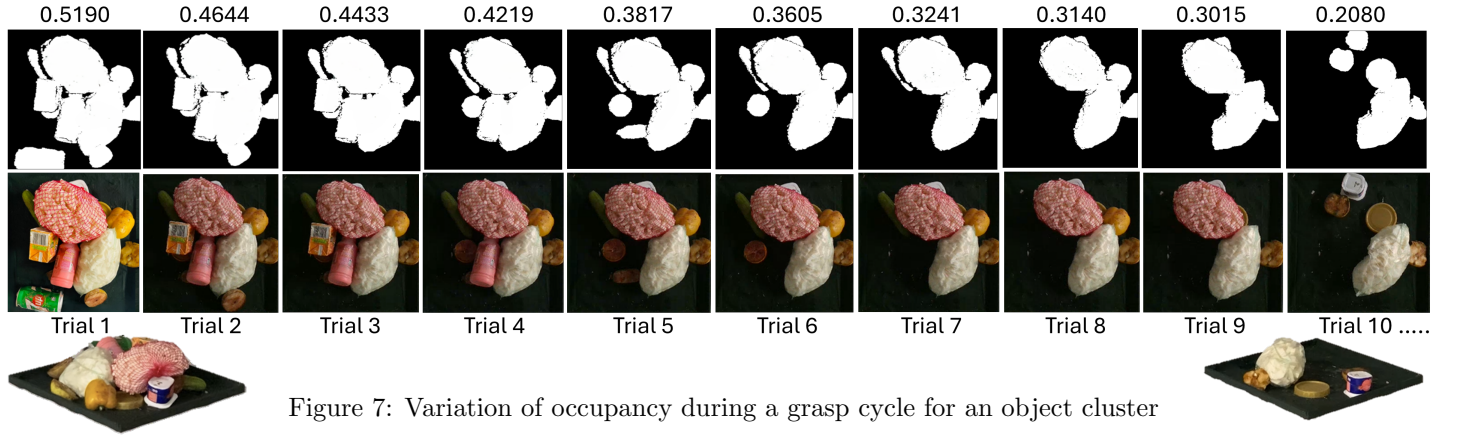


Figure 7: Variation of occupancy during a grasp cycle for an object cluster

valid object points to a predefined range of 250–525 mm to exclude noise and background pixels outside the graspable region. Finally, occupancy was computed as the ratio of object pixels (passing all filters) to the total workspace pixels, expressed as a percentage.

3.2.2 Grasp Performance Metrics

While graspability parameters assess an object’s ability to be grasped, grasp performance metrics evaluate the effectiveness of the grasping modes, the grippers. In our framework, grasp performance is measured not only by grasp success but also by grasp stability and efficiency.

Grasp Success Score (S_p) :

This metric defines the execution success of a grasp trial and is given by

$$S_p = \begin{cases} 1, & \text{if the object is grasped and successfully moved to the pre-grasp pose} \\ 0.5, & \text{if the object is grasped but dropped while moving to the pre-grasp pose} \\ 0, & \text{otherwise.} \end{cases} \quad \text{Equation (10)}$$

Grasp Stability Score (S_b):

This score measures how stable the grasp remains during a successful execution. It reflects the gripper’s ability to securely hold the object while moving it from the grasp pose to the drop pose. To evaluate this, we implemented an object-holding tracking system for all three grippers. For the rigid and Fin-Ray grippers, force sensors (FSR UX-400 and FSR UX-408, respectively) were embedded by modifying the finger mounts and calibrated accordingly (Figure 3). The sensor actuation circuitry was controlled via a relay module integrated with an Arduino microcontroller, with communication managed through ROS 2 (Figure 2).

The functionality of the sensing system follows a layered process: once the robot reaches the grasp pose, the relay-control node in the ROS 2 control stack activates the sensor by sending a switching signal through the Arduino. The sensor is deactivated similarly once the robot reaches the drop pose (end-point). The sensor continuously records force readings from the grasp pose through to the drop pose. If the object is dropped mid-way due to slippage during transport, the sensor detects a reduction of force to zero. The stability score, $S_b \in [0, 1]$, is then defined as the ratio of the time interval from the grasp point (t_1) to the drop point (t_2) over the total expected holding time from the grasp point (t_1) to the end point (t_3) (Figure 8):

$$S_b = \begin{cases} 1, & \text{if the object is held securely until the end point } (t_2 = t_3) \\ \frac{t_2 - t_1}{t_3 - t_1}, & \text{if the object is dropped mid-way at time } t_2 \end{cases} \quad \text{Equation (11)}$$

Similarly, in the case of the suction gripper, the relay circuit is used to control the Honeywell APB pressure sensor, which records negative pressure at defined time intervals to assess grasp stability.

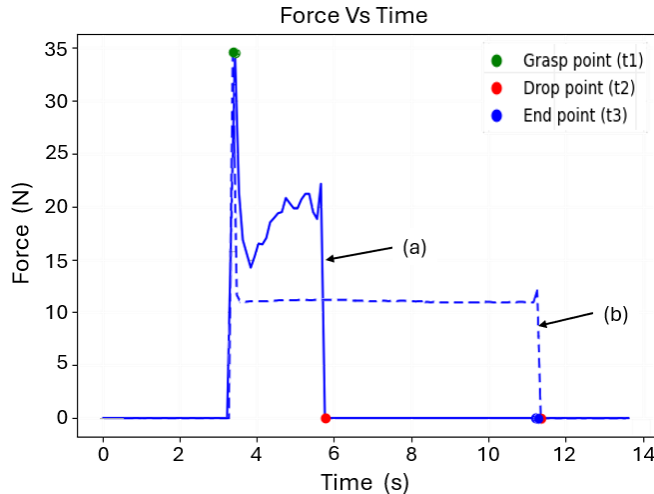


Figure 8: Sensor readings for stability measurement: (a) case where the object is dropped mid-way due to slippage, (b) case where the object is successfully transferred from the grasp pose to the drop pose (end point).

Grasp Efficiency Score (S_f):

The efficiency score measures how effectively a grasping cycle is executed. It is determined by the time required to complete the full cycle, starting from the pre-grasp position and ending with the release of the object at the drop point. To ensure consistency, the average cycle time across all successful trials in an experiment is calculated and then normalized to produce the efficiency score. This metric captures not only the speed of execution but also reflects the overall responsiveness of the grasping system.

$$S_f = 1 - \frac{T_c - T_{\min}}{T_{\max} - T_{\min}} \quad \text{Equation (12)}$$

where T_c is the grasp cycle time of the trial, T_{\min} is the minimum cycle time across successful trials for a experiment, and T_{\max} is the maximum cycle time across successful trials for a experiment, with $S_f \in [0, 1]$.

Overall, this benchmarking framework provides a means to examine how Pre-grasp conditions influence the performance of robotic grasping in food waste sorting. In particular, three graspability parameters grasp score Q_p , object score Q_o , and clutter score Q_c are evaluated in relation to three performance measures: grasp success S_p , grasp stability S_b , and grasp efficiency S_f . The evaluation considers not only how variations in these parameters affect grasping outcomes but also how performance differs across object categories, thereby identifying opportunities for cross-category implementation of grasping modalities.

4 Experimental Procedure

The benchmarking framework followed a structured experimental procedure, assessing grasp performance across four levels of increasing complexity. These experiments enabled us to highlight critical limitations and the need for the given grasping modalities.

4.1 Experiment 1 – Scene with a Single Inorganic Object

The experimental series was designed to follow a progression of increasing clutteriness. As a baseline, the first experiment focused on grasping a single object placed within the scene, where the scene refers to the workspace area captured by the vision system. In this setup, each object from the dataset was randomly positioned in five distinct locations within the workspace, and grasp attempts were performed accordingly. For each object category, this produced 15 trials (3 objects \times 5 positions). In total, 105 trials were conducted across all seven categories for a single grasping mode, and 315 trials overall when repeated with all three gripper modalities. During every trial, all six evaluation metrics, including the graspability parameters and grasp performance metrics, were systematically recorded. One important observation, discussed further in Section 5, is that the mean success score for the plastic bag and mesh bag categories with the suction gripper was zero. This reflects a systematic limitation of suction-based grasping, where

the inability to form a stable seal on highly deformable or porous objects leads to air leakage and poor surface conformity, thereby preventing successful grasps. Consequently, in the subsequent cluttered-scene experiments, these two categories were excluded from the suction gripper evaluation.

4.2 Experiment 2 – Inorganic Objects in Medium-Clutter Scene

The second experiment increased the clutter level of the scene by introducing seven objects at a time. Using the full dataset, three clusters were created, each containing seven objects with representation from all categories, while a controlled version with five objects was used for the suction gripper assessment. Objects in each cluster were randomly arranged within the workspace to replicate cluttered conditions. For each cluster, seven consecutive grasp attempts were carried out, selecting the highest-ranked pose from the top eight poses generated by AnyGrasp or SuctionNet after post-processing. Each cluster was repeated five times, yielding 105 trials for both the rigid and Fin-Ray grippers (7 objects \times 5 attempts \times 3 clusters) and 75 trials for the suction gripper (5 objects \times 5 attempts \times 3 clusters). Across all three gripper modalities, this amounted to 285 trials in total. The same evaluation metrics, graspability parameters and grasp performance measures were applied consistently throughout.

4.3 Experiment 3 – Inorganic Objects in High-Clutter Scene

In the third experiment, we increased the clutteriness to high by introducing 14 objects for a scene (This appeared to be the maximum accompanied within the workspace boundaries and vision-related optimal depth ranges). In these experiments, clusters developed in the third experiment were mixed two at a time and prepared the group of 14 objects for a scene and then randomly placed in the workspace. Each group contained two representatives from each category, except for the suction gripper, where two categories were excluded, resulting in 10 objects per scene. For each group, 14 consecutive grasp attempts were carried out, following the same procedure as in Experiment 2. Each group was tested over five repetitions, yielding a total of 210 trials for the rigid and Fin-Ray grippers (14 objects \times 5 attempts \times 3 groups) and 150 trials for the suction gripper (10 objects \times 5 attempts \times 3 groups). Across all three gripper modalities, this amounted to 570 trials in total. Same evaluation metrics, graspability parameters and grasp performance measures were recorded for the evaluation.

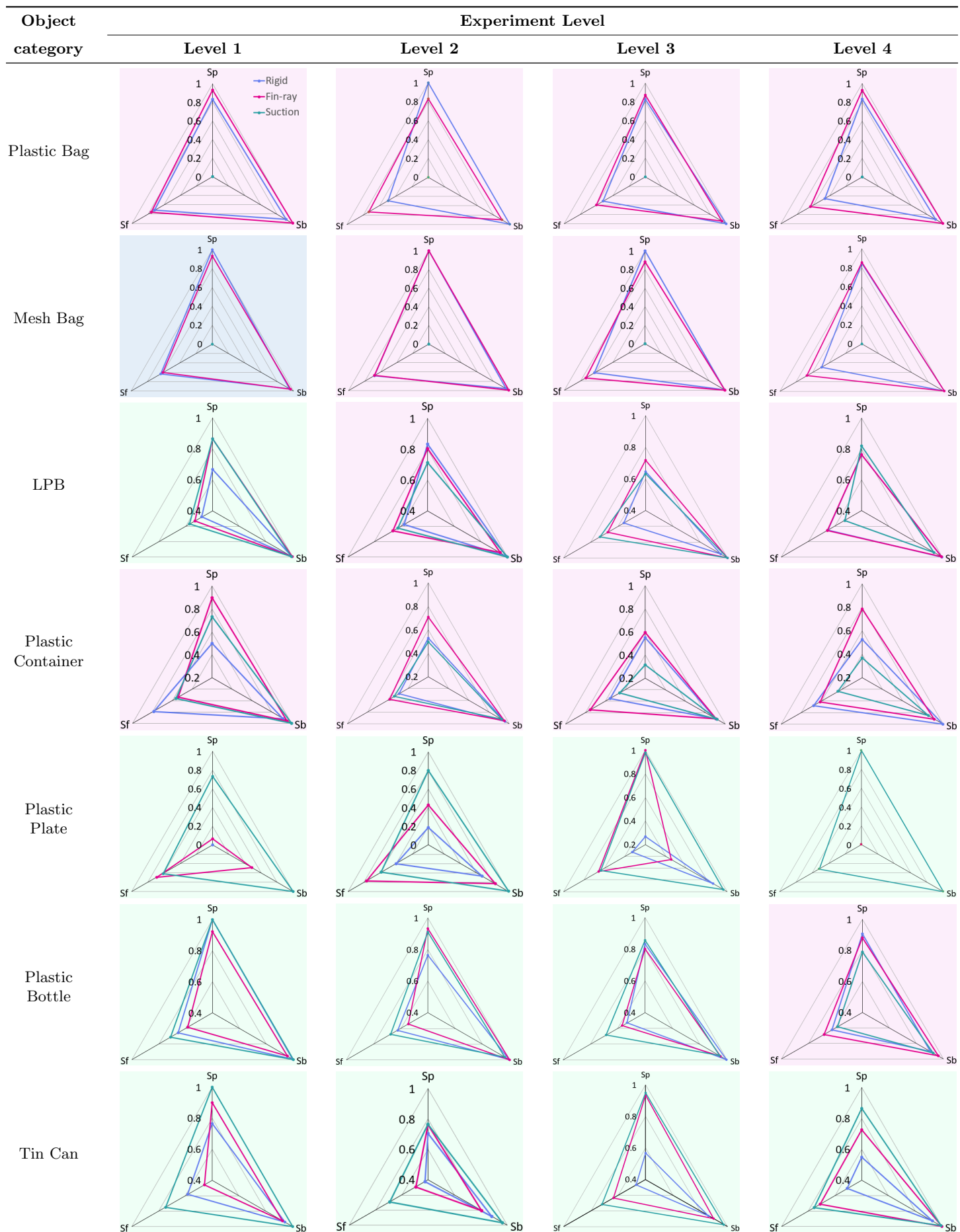
4.4 Experiment 4 – High-Clutter Mixed Food Waste Scene

The final experiment was designed to replicate realistic food waste sorting conditions by combining seven inorganic objects with seven organic food waste items, resulting in a total of 14 objects per scene. This mixed setup introduced additional challenges such as occlusions, adhesion on sticky surfaces, variable textures, including thin watery layers forming between the gripper surface and the object and entanglement effects, all of which reflect industrial conditions within a controlled laboratory environment. Following the same procedure as in Experiment 3, objects were randomly distributed in the workspace, and 14 consecutive grasping cycles were performed, each targeting a single object, with the exception applied to the suction gripper as noted previously. The complete grasping pipeline was executed across all three gripper modalities, yielding a total of 570 trials for evaluating performance in these heterogeneous scenes.

5 Results and Discussion

The results analysis is presented in three phases. First, we compare the grasp performance of the three unimodal grippers across four high-fidelity experiments and object categories. Second, we analyse how pre-grasp conditions, expressed through graspability parameters, influence performance in each gripper modality. Finally, we examine failure occurrence rates and assess the impact of graspability parameters on different failure modes.

Table 1: Evaluation of grasp performance using radar charts. Performance polygons are color-coded by gripper (blue: rigid, pink: Fin-Ray, green: suction), where the gripper with the largest enclosed area represents the highest overall performance, indicated by the corresponding background color.



5.1 Performance Comparison of Grasping Modalities

Based on the performance scores for three metrics, we use a radar chart to visualize and compare the performances of different grippers overall as well as object category-wise in 4 levels of experiments (Table 1). The radar chart has three axes, representing grasp success S_p , grasp stability S_b , and grasp efficiency $S_f \in [0, 1]$. For each experimental level, category-wise mean scores were computed and plotted on the corresponding axes. Connecting these points forms a polygon that illustrates the overall performance profile of each gripper. A vertex positioned at the centre of the chart indicates a score of zero on that axis, whereas outward extensions represent higher scores. In some cases, the axes are contracted rather than starting strictly at zero, to better highlight relative differences between grippers.

The interpretation of the performance comparison is summarized as follows:

Experiment 1 Analysis of the radar chart polygons revealed that the Fin-Ray gripper achieved the best performance with plastic bags and plastic containers, while the rigid gripper excelled only in mesh bags. In contrast, the suction gripper showed the lowest performance in these deformable categories, with plastic bags and mesh bags yielding zero success due to non-conforming surfaces that prevented suction sealing. A noteworthy observation, however, is that in single-object scenarios, the suction gripper outperformed the other grippers in four out of seven categories (laminated paper boxes (LPB), plastic plates, plastic bottles, and tin cans), highlighting its suitability for flat, rigid surfaces. In these categories, the other two grippers showed reduced success, and the rigid gripper in particular recorded zero success for plastic plates due to collisions with the base when the object was positioned too close to the surface (further explained in 5.3).

Experiment 2 and 3 Both the medium and high clutter experiments (7 objects and 14 objects per scene, respectively) demonstrated similar overall performance despite the increase in scene complexity. Among the seven object categories, the Fin-Ray gripper outperformed in four plastic bags, mesh bags, laminated paper boxes (LPB), and plastic containers. The corresponding radar charts indicate that while both the rigid gripper and the Fin-Ray gripper performed similarly in these categories, the Fin-Ray consistently outperformed the rigid gripper due to its excellent shape-morphing capability, which adapts effectively to varying object surfaces. However, both grippers exhibited very low overall performance on flat and rigid surfaces. Consistent with the results from the non-cluttered scenario (single object grasping), the suction gripper achieved the highest overall performance in plastic plates, plastic bottles, and tin cans, the three categories characterized by high rigidity and flat surface structures.

Experiment 4 In the mixed food waste scenario, the Fin-Ray gripper achieved the highest overall success, outperforming the other two grippers and demonstrating greater tolerance to the additional challenges introduced by organic waste. This superior performance was observed across five of the seven categories: plastic bags, mesh bags, laminated paper boxes (LPB), plastic containers, and plastic bottles. For the rigid and suction grippers, most failures were caused by slipping, as the liquid nature of the environment reduced the coefficient of friction and increased the likelihood of slip in their small contact regions. In contrast, the Fin-Ray gripper maintained a larger region of contact due to its shape-morphing property, which enhanced stability under these conditions. A notable observation is that while the suction gripper outperformed in plastic bottles during inorganic cluttered scenes (Experiments 2 and 3), the advantage shifted to the Fin-Ray gripper in the mixed waste scene, highlighting the suction gripper’s inability to tolerate varying object geometries and fluidic conditions that disrupt suction. Nevertheless, consistent with other cluttered experiments, the suction gripper still excelled in plastic plates and tin cans, benefiting from its strong conformance on smooth, thin flat surfaces, despite disturbances caused by thin liquid films between the suction cup and object surfaces.

Overall, despite the challenges posed by cluttered scenes, the adaptive Fin-Ray gripper demonstrated the highest resilience when handling deformable to semi-deformable objects plastic bags, mesh bags, laminated paper boxes, plastic containers, and plastic bottles indicating strong cross-category suitability for the given

use case. In particular, the radar chart results for Experiment 4 show that it outperforms the other two grippers when dealing with the sticky and irregular nature of food-waste scenarios. However, the Fin-Ray gripper showed lower resilience with objects that had thin, flat surfaces (plastic plates and tin cans), where frequent collisions with the work base became a significant issue due to the stiffness of its fingertips. In contrast, for these object categories, the suction gripper exhibited the highest adaptability, owing to its strong conformance with flat surfaces and its top-down approach. Unlike the rigid and Fin-Ray grippers, which operate in parallel to the work surface, the suction gripper’s vertical approach minimizes base collisions, making it particularly effective for thin, flat objects.

5.2 Effect of Graspability on Grasp Performance

In this phase, we analyze how pre-grasp conditions (graspability parameters), which emerged as the main predictors of grasp performance, influence performance in each gripper modality. We use inferential modeling to explain and quantify how the predictors, grasp score Q_p , object score Q_o , and clutter score Q_c impact the three independent outcomes: grasp success S_p , grasp stability S_b , and grasp efficiency S_f . As the first step, we conducted Exploratory Data Analysis (EDA) to understand the suitability of the models for the obtained results. We examined the distributions of the graspability parameters using histograms and correlation density plots. The predictors show non-normal but only mildly skewed distributions and are already represented on an interpretable $[0,1]$ scale. Correlations between predictors are low ($|r| < 0.33$), indicating no multicollinearity; therefore, logistic-based models are preferred over linear models.

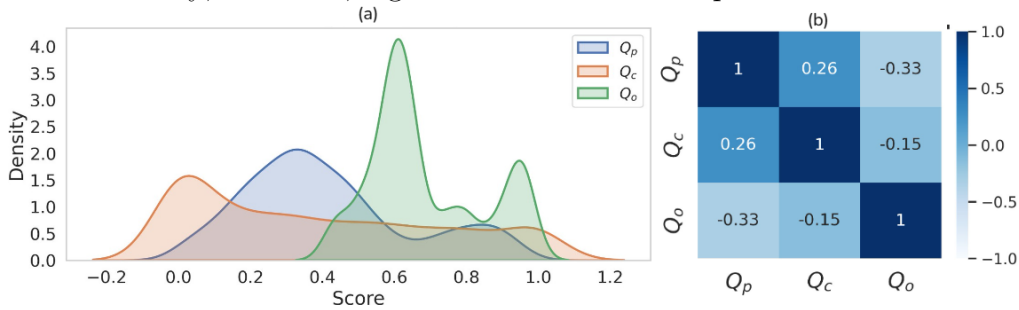


Figure 9: Exploratory data analysis of graspability parameters. (a) Kernel density distributions of object score Q_o , grasp score Q_p and clutter score Q_c (b) Correlation matrix showing low pairwise correlations ($|r| < 0.33$)

In our dataset, S_p serves as a binary indicator, while S_b , and S_f are continuous rates constrained within $[0, 1]$. Accordingly, each outcome is modeled using a logit link appropriate to its scale: S_p is fit with a standard logistic regression [41] whereas S_b and S_f are modeled using a fractional logit regression that explicitly accounts for the fractional nature of the dependent variable [42]. The same set of predictors is used across all three models: Q_O , Q_P and Q_C with gripper type included as a categorical factor, $C(\text{Gripper_type})$, where Rigid is set as the reference (baseline) category. Interactions between each graspability parameter and gripper type are also incorporated. Formally, for each outcome $S_k \in \{S_P, S_B, S_F\}$, the model is expressed as

$$g_k(\mathbb{E}[S_k]) = \beta_{0,k} + \beta_{O,k}Q_O + \beta_{C,k}Q_C + \beta_{P,k}Q_P + C(\text{Gripper_type}) + (Q_O + Q_C + Q_P):C(\text{Gripper_type}) \quad \text{Equation (13)}$$

The function $g_k(\cdot)$ denotes the appropriate link function applied to the expected value of each outcome. The interaction terms ($\beta_{O,k}Q_O$, $\beta_{C,k}Q_C$ and $\beta_{P,k}Q_P$) are essential, as they allow the effects of graspability parameters to differ across gripper types with respect to baseline. For example, the benefit of improved pose quality may be greater for suction than for rigid (the baseline), rather than being restricted to a common slope across all grippers. We deliberately exclude the experimental level factor from the mean model. Level is a coarse design factor that largely proxies aspects already measured continuously by the graspability parameters Q_O , Q_P , and Q_C . For all three outcomes, we report regression coefficients, their exponentiated form (odds ratios), p-values, and 95% confidence intervals. For binary success S_p , the odds ratios have the usual interpretation in terms of odds of success. For stability S_b and efficiency S_f , which are

Table 2: Effects of graspability parameters across performance measurements. Green = significant positive ($p < 0.05$), Red = significant negative ($p < 0.05$), White = not significant.

Term	S_p			S_b			S_f		
	coef	OR	p	coef	OR	p	coef	OR	p
Q_P	3.7457	42.340	0.017	3.7656	43.188	0.011	1.7003	5.476	0.076
Q_C	0.5524	1.737	0.334	0.4505	1.569	0.413	0.1008	1.106	0.719
Q_O	4.6109	100.571	0.000	4.4530	85.885	0.000	2.2798	9.775	0.003
Finray vs Rigid	1.3412	3.824	0.032	1.1100	3.034	0.048	0.9061	2.475	0.049
$Q_P \times$ Finray	-0.0215	0.979	0.984	-0.1245	0.883	0.896	-0.3935	0.675	0.535
$Q_C \times$ Finray	-0.1135	0.893	0.859	0.0512	1.053	0.933	0.0489	1.050	0.867
$Q_O \times$ Finray	-1.1672	0.311	0.176	-0.9245	0.397	0.268	-0.7718	0.462	0.211
Suction vs Rigid	9.7571	17275.970	0.000	10.0291	22677.748	0.000	5.4588	234.809	0.000
$Q_P \times$ Suction	-2.8253	0.059	0.085	-2.8407	0.058	0.064	-0.8290	0.436	0.445
$Q_C \times$ Suction	-1.5892	0.204	0.077	-1.6894	0.185	0.073	-0.7217	0.486	0.111
$Q_O \times$ Suction	-12.9050	0.000	0.000	-13.1573	0.000	0.000	-7.7226	0.000	0.000

fractional outcomes, the odds ratios describe multiplicative effects on the odds of the expected proportion.

Considering the odds ratios and p-values (Table 2) from the regression models, in overall, the Finray (refer to raw *Finray vs Rigid*) and Suction (refer to raw *Suction vs Rigid*) grippers show extremely strong performance relative to the Rigid baseline ($p < 0.05$). This pattern is consistent with quasi-complete separation, indicating that both Fin-ray and Suction almost always succeed under the evaluated conditions. For grasp success S_p object quality Q_O emerges as the dominant driver for the rigid (refer to raw Q_O) and suction gripper (refer to raw $Q_O \times Suction$). For rigid higher Q_O significantly increases the odds of a successful grasp ($p = 0.017 < 0.05$). In contrast, for the Fin-ray gripper, the effect of Q_O is weak whereas for the Suction gripper, shows a strong negative association. The pose quality score Q_P also contributes positively to success for the Rigid gripper (refer to raw Q_P), though it does not reach significance for either Fin-ray (refer to raw $Q_P \times Finray$) or Suction (refer to raw $Q_P \times Suction$). Across all three grippers, the clutter metric Q_C shows no clear average effect on success. The effects on stability S_b largely mirror those observed for success. For the rigid gripper, Q_O is again the strongest positive predictor, and Q_P also shows a significant positive effect. However, Q_C remains non-significant for grippers. This suggests that the quantified clutter measure contributed only weakly to explaining performance variability, or that its effect may be partially absorbed by other predictors in the model. For efficiency S_f , the pattern is similar to that of success and stability. Q_O remains a strong positive predictor for the rigid gripper, is not significant for the fin-ray, and shows a strongly negative effect for the suction gripper. Other than this, efficiency does not appear to strongly depend on graspability parameters and may instead be influenced by factors such as the advancement of path planning and control algorithms.

To visualize these effects, we further generated partial dependence plots (PDPs) (Figure 10) for each outcome against each graspability parameter. These PDPs show the relationship between a graspability parameter and the expected outcome, separately for each gripper, while integrating over the empirical distribution of the remaining factors. The object score (Q_O), representing the object-quality pre-grasp condition, positively influences success, stability, and efficiency, showing a strong increase in performance as Q_O rises for the fin-ray and rigid gripper. In contrast, the rigid gripper exhibits only a modest positive trend, while the suction gripper shows a pronounced negative slope across all outcomes, confirming that higher Q_O (highly deformable objects) reduces performance for suction. For pose quality (Q_P), a clear positive effect is observed for the rigid gripper on success, stability, and efficiency though the effect is moderate for fin-ray and absent for suction. Finally, clutter (Q_C) shows no strong or consistent effect for rigid and fin-ray grippers, with relatively flat or slightly positive trends, whereas suction consistently shows a negative relationship across all outcomes, indicating degraded performance as clutter increases.

5.3 Failure Mode Analysis

In addition to analyzing grasp performance and its relationship with graspability parameters, we also examined the failure cases in the third phase. This analysis focused on identifying the most frequent types of failure modes across the three gripper modalities and understanding how graspability parameters (pre-

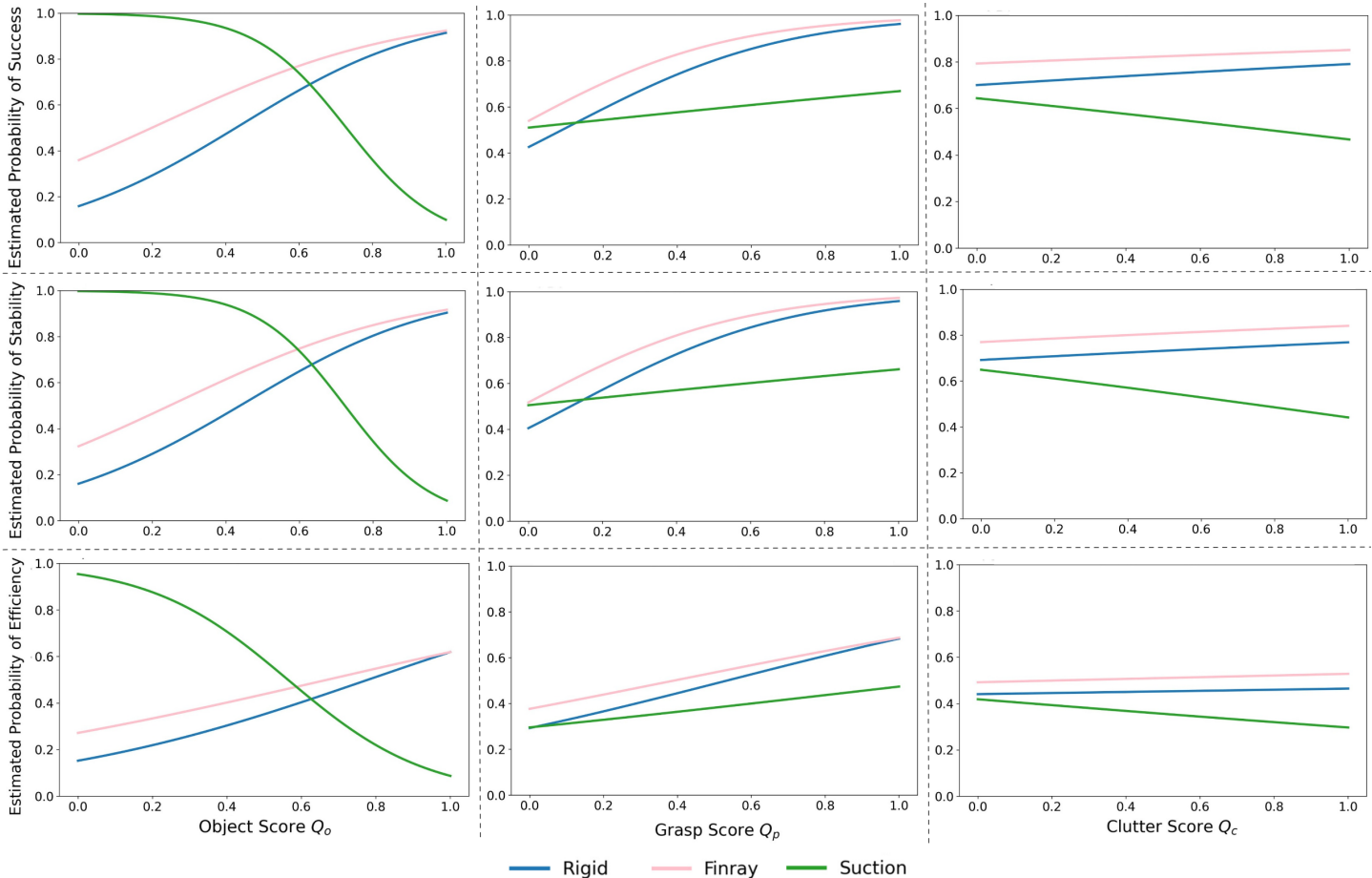


Figure 10: Partial dependence plots illustrating the relationship between graspability parameters (Object Score Q_o , Grasp Score Q_p , and Clutter Score Q_c) and performance metrics (Grasp Success S_p , Grasp Stability S_b and Grasp Efficiency S_f) for the three gripper types.

grasp conditions) contribute to the occurrence of failures. We categorized failure modes into three major categories: physical interaction failures, perception failures, and execution failures. Physical interaction failures included gripper collisions with the work base or targeted object (CL), collisions with surrounding objects (CLS), slippage (SL), and failures related to object properties such as non-planar or highly irregular surfaces (OP). Perception failures primarily involved grasp pose misalignment due to incorrect pose generation by the vision system (WGP). Execution failures referred to errors arising during the grasp control process that prevented the successful completion of the grasp cycle.

5.3.1 Frequency of Grasp Failure Occurrence

As shown in Figure 11 (a), physical interaction failures accounted for more than 70% of the total failure cases across all three grippers, highlighting that improvements in the physical design of grippers are essential. Perception failures represented 11%, 22%, and 28% of the failures for the rigid, Fin-Ray, and suction grippers, respectively, indicating that the state-of-the-art grasp pose detection methods employed in the system contributed reasonably well to grasp evaluation by limiting vision-related errors. Execution failures constituted less than 1% of the total cases and occurred only with the Fin-Ray gripper, which highlights the high accuracy and reliability of the ROS-based path planning algorithm integrated into the benchmarking pipeline.

As physical interaction failures accounted for more than 70% of the total, these categories were analyzed in greater detail (Figure 11(b)). For the rigid and Fin-Ray grippers, collisions with the work base or the targeted object (CL) were the most frequent, occurring in over 60% of cases. These failures typically involved the fingertip colliding with either the base surface or the object itself, highlighting the need to improve fingertip flexibility to reduce such cases. In contrast, for the suction gripper, object property-related failures (OP) represented the highest proportion of physical interaction failures. These were mainly

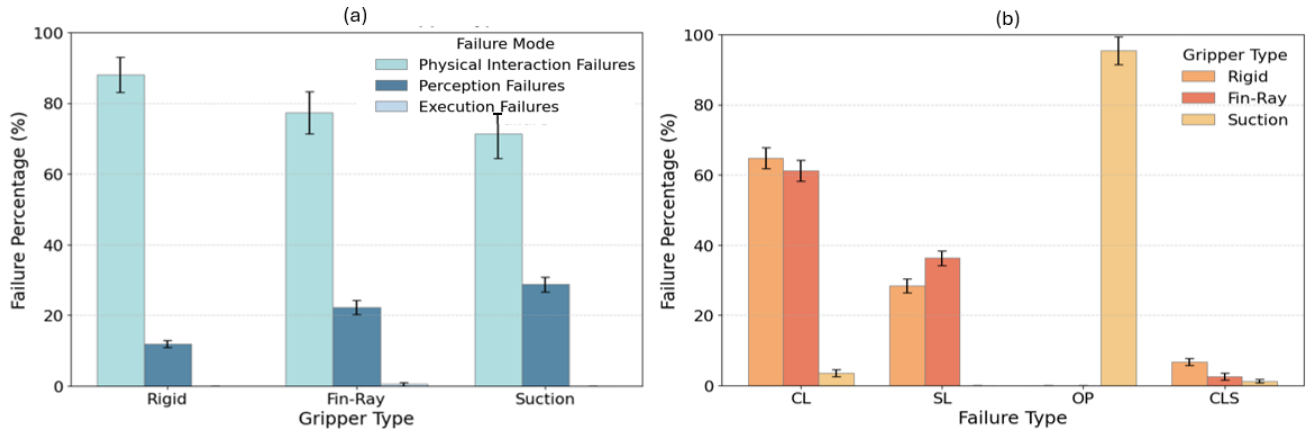


Figure 11: (a) Variation in three major categories of failure modes: physical interaction failures, perception failures, and execution failures observed across the three grasping modalities. (b) Variation of physical interaction failure types: CL - gripper collisions with the work base or target object, CLS - collisions with surrounding objects, SL - slippage, and OP - failures associated with object properties such as non-planar or highly irregular surfaces.

caused by the inability of the suction cup to conform to varying object surfaces, particularly under fluidic conditions that closely resemble real food waste sorting environments. This indicates the importance of redesigning the suction cup to better accommodate adversarial object properties and environmental conditions, as OP accounted for nearly 95% of suction failures.

Additionally, slipping (SL) was the second most significant physical interaction failure for both the rigid and Fin-Ray grippers, contributing to more than 25% of total failures in each case. This suggests the need to improve the coefficient of friction at the gripper’s contact surfaces. Meanwhile, collisions with surrounding objects (CLS) were relatively rare, at less than 10% across all gripper modalities, underscoring the accuracy of grasp pose generation provided by the selected vision models.

5.3.2 Impact of Graspability Parameters on Grasp Failure Occurrence

The second stage of the failure analysis involves identifying the impact of pre-grasp conditions, or graspability parameters, for the observed failure cases. In this context, the object score Q_O , grasp score Q_P and clutter score Q_C emerged as predictors for the failure modes CL, CLS, SL, OP, and WGP, helping to explain which pre-grasp condition contributes most to each type of failure. The box plots in Figure 12 compare the influence of these pre-grasp measures on different failure modes across grippers, and the overall effects are summarized in Table 3.

For rigid and Fin-Ray grippers, collisions with the work base or the target object (CL) were common when the object score was low, as with rigid items such as plastic containers, plates, or bottles, but not with deformable objects like plastic bags. This strengthens the argument made in Section 5.3.1, highlighting the need for fingertip flexibility. CL was also linked with lower grasp pose quality, which is expected since AnyGrasp and SuctionNet both generate grasp scores based on collision-aware models. However, clutter did not appear to be the main driver of CL, reinforcing the interpretation that fingertip flexibility is the critical factor. For rigid and Fin-Ray grippers, collisions with surrounding objects (CLS) showed a trend similar to CL with respect to object score. More importantly, CLS displayed the strongest dependency on clutter, consistently increasing under high Q_C and low grasp scores Q_P . Notably, CL, CLS, and SL were not observed for the suction gripper.

In the rigid and Fin-Ray grippers, slip-related failures (SL) occurred across moderate-high Q_C values, with a wide spread of clutter, suggesting that factors beyond clutter play a role. This indicates that improving the contact surfaces of the gripper could help mitigate such failures. Grasp pose misalignment (WGP) failures across all three grippers were associated with higher Q_O corresponding to deformable objects. This suggests that the grasp pose generation models used in the system were not adequately trained for highly deformable objects, highlighting the need for such contributions in food waste sorting applications.

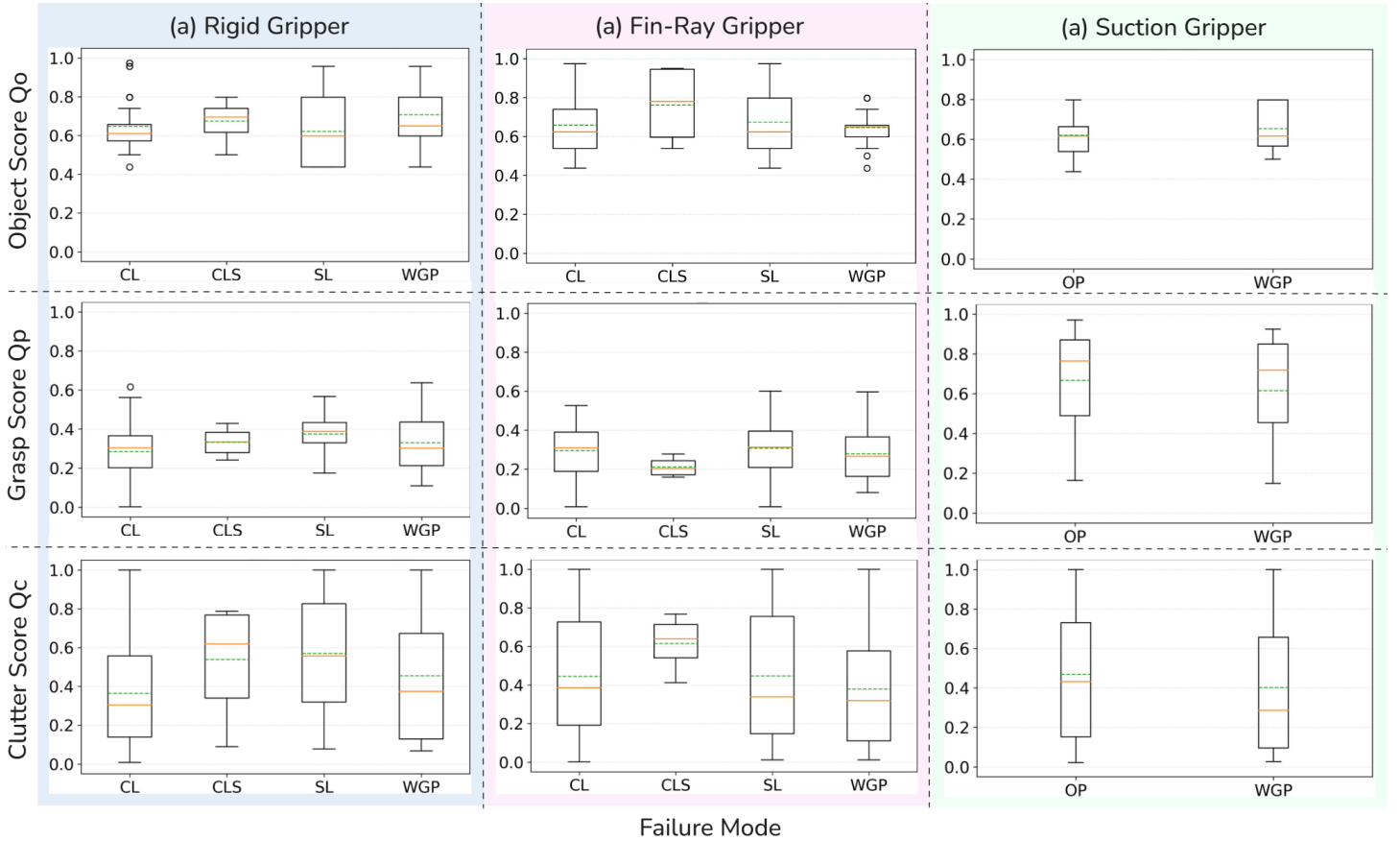


Figure 12: Impact of graspability parameters (pre-grasp conditions) Q_O , Q_P and Q_C on the occurrence of grasp failures for three gripper modalities: (a) rigid two-finger parallel gripper (RG2) (b) soft adaptive two-finger Fin-Ray gripper (c) Suction Gripper

However, WGP failures did not show a significant relationship with grasp pose quality. Instead, they appear to be more influenced by the training of the grasp pose generation and the effectiveness of the grasp pose selection process. Notably, WGP failures were not clutter-driven. Finally, object property-related failures (OP) were unique to the suction gripper. They appeared across all object categories, and unlike the other modes, OP failures increased even under high Q_P , while clutter showed only a moderate influence.

Table 3: Impact of object-related (Object Score Q_O), grasp quality-related (Grasp Score Q_P), and clutter-related (Clutter Score Q_C) pre-grasp conditions on the occurrence of failure modes across gripper types (corresponding to Fig. 12).

	Failure Mode	Q_O (Object Score)	Q_P (Grasp Score)	Q_C (Clutter Score)
Rigid / Fin-Ray	CL	✓	✓	×
	CLS	✓	✓	✓
	SL	△	△	△
	WGP	✓	△	×
Suction	WGP	✓	△	×
	OP	✓	△	△

✓: strong influence; △: moderate influence; ×: weak or no influence.

6 Conclusions

We presented GRAB, a comprehensive benchmarking framework for evaluating robotic grasping in food-waste sorting environments. The primary strength of GRAB lies in its novel integration of object, vision, and environment-related pre-grasp conditions through established graspability metrics, providing a principled basis for analyzing grasp behaviour under realistic operational conditions.

Our investigation into the grasp performance of industrial grippers across seven contaminant categories, visualized via radar charts, reveals a clear performance dichotomy. The Fin-Ray gripper demonstrated superior resilience when handling deformable to semi-deformable objects, which constitute approximately 92% of inorganic contaminants in food waste, consistently outperforming both the rigid and suction grippers. However, its performance was lowest on flat, thin-surfaced objects, which represent the remaining 8% of contaminants. For these specific categories, the suction gripper achieved the highest overall performance, showing greater tolerance and effectiveness on rigid, planar surfaces. This stark division in gripper efficacy indicates a crucial practical requirement, the integration of multiple modalities into a single, multi-modal gripper is necessary to achieve robust cross-category applicability in food waste sorting.

Further investigations, which encompass the statistical analysis on the effect of graspability on grasp performance, demonstrate that the object score Q_O is the dominant positive predictor for success, stability, and efficiency in both the Fin-Ray and rigid grasping modalities. In contrast, Q_O negatively impacts suction-based grasping compared to the other predictors. This highlights the importance of incorporating object quality into the design considerations when developing cross-category capable robotic grippers, as it strongly influences grasp outcomes and failure behaviour.

From the grasp pose quality Q_P , a strong positive effect is observed for rigid gripper performance, while the effect is moderate for the Fin-Ray gripper. This indicates that rigid grippers rely on accurate pose alignment to achieve force closure and stable contact, whereas the compliance of Fin-Ray fingers can partially compensate for pose inaccuracies. This difference in dependence on precise alignment across gripper modalities highlights the need for gripper modality specific vision strategies.

From the failure mode analysis, it is noted that over 70% of failures arise from physical interaction, including collisions with the work base or targeted object and slipping. These failures are strongly linked to variation in object quality and grasp pose accuracy, indicating the importance of incorporating structural flexibility and improved surface contact as key design factors for future gripper development. Meanwhile, improved vision models specifically trained on food waste scenarios can help generate accurate grasp poses for specific object categories. In contrast, suction failures were driven by object property challenges and fluidic disturbances, demonstrating the need for improved suction sealing strategies and robustness under adverse environmental conditions.

Overall, GRAB is shown to be a promising and useful framework for evaluating grasp performance not only in food waste sorting but also in other multi-object-category grasping scenarios. It supports identifying and selecting grasping modality while providing a clear understanding of how pre-grasp predictors influence overall performance.

Supporting Information

Supporting Information is available from the Wiley Online Library or from the author.

Acknowledgements

This work was jointly funded by a PhD scholarship awarded to Moniesha Thilakarathna from the University of Canberra and GOTERRA PTY LTD.

References

- [1] J. Pickin, C. Wardle, K. farrell, L. Stovell, P. Nyunt, S. Guazzo, Y. Lin, G. Caggiati-Shortell, P. Chakma, C. Edwards, B. Lindley, G. Latimer, J. Downes, I. Axio, and R. Reviewers, "National waste report 2022," 12 2022.
- [2] NSW Environment Protection Authority, "Emissions impacts of food waste recovery technologies," 2022. [Online]. Available: <https://www.epa.nsw.gov.au>
- [3] Y.-H. Lin, w.-l. Mao, and H. I. K. Fathurrahman, "Development of intelligent municipal solid waste sorter for recyclables," *Waste management (New York, N.Y.)*, vol. 174, pp. 597–604, 12 2023.

- [4] C. Lubongo, M. A. B. Daej, and P. Alexandridis, “Automated sorting technology for plastic waste,” in *Reuse of Plastic Waste in Eco-Efficient Concrete*. Elsevier, 2024, pp. 13–35.
- [5] Z. Long, Q. Jiang, T. Shuai, F. Wen, and C. Liang, “A systematic review and meta-analysis of robotic gripper,” *IOP Conference Series: Materials Science and Engineering*, vol. 782, 2020, 4.4.
- [6] J. Mahler, R. Platt, A. Rodriguez, M. Ciocarlie, A. Dollar, R. Detry, M. A. Roa, H. Yanco, A. Norton, J. Falco, K. v. Wyk, E. Messina, J. Leitner, D. Morrison, M. Mason, O. Brock, L. Odhner, A. Kurenkov, M. Matl, and K. Goldberg, “Guest editorial open discussion of robot grasping benchmarks, protocols, and metrics,” *IEEE Transactions on Automation Science and Engineering*, vol. 15, no. 4, pp. 1440–1442, 2018.
- [7] T. Lerher, P. Bencak, D. Hercog, B. Jerman, and L. Bizjak, “Robotic bin-picking: Benchmarking robotics grippers with modified ycb object and model set,” in *Proceedings of the 16th Progress in Material Handling Research*. Dresden, Germany: University of Maribor and University of Ljubljana, Jun. 2023, presented at Summer 6–21, 2023.
- [8] N. Fangerow, N. Basedow, and D. Aschenbrenner, “Development of a benchmarking system for the evaluation of robot grippers for their suitability in the field of sorting post-consumer plastics,” *Procedia CIRP*, vol. 130, pp. 890–896, 2024, 57th CIRP Conference on Manufacturing Systems 2024 (CMS 2024). [Online]. Available: <https://www.sciencedirect.com/science/article/pii/S2212827124013386>
- [9] Z. Qiu, H. Paul, Z. Wang, S. Hirai, and S. Kawamura, “An evaluation system of robotic end-effectors for food handling,” *Foods*, vol. 12, no. 22, p. 4062, Nov. 2023.
- [10] T. Chen, R. Frumento, G. Pagnanelli, G. Cei, V. Keth, S. Gafarov, J. Gong, Z. Ye, M. Baracca, S. D’Avella, M. Bianchi, and Y. Sun, “Benchmarking multi-object grasping,” *IEEE Robotics and Automation Letters*, vol. 10, no. 9, pp. 9510–9517, 2025.
- [11] J. Falco, D. Hemphill, K. Kimble, E. Messina, A. Norton, R. Ropelato, and H. Yanco, “Benchmarking protocols for evaluating grasp strength, grasp cycle time, finger strength, and finger repeatability of robot end-effectors,” *IEEE Robotics and Automation Letters*, vol. 5, no. 2, pp. 644–651, 2020.
- [12] F. Bottarel, G. Vezzani, U. Pattacini, and L. Natale, “Graspa 1.0 : Graspa is a robot arm grasping performance benchmark,” *IEEE Robotics and Automation Letters*, vol. PP, pp. 1–1, 01 2020.
- [13] M. Thilakarathna, X. Wang, A. Wijesinghe, D. Hinwood, and D. Herath, “Robotic grasping for automated sorting of complex, highly contaminated industrial food waste: A benchmark study,” in *2025 IEEE/RSJ International Conference on Intelligent Robots and Systems (IROS)*, 2025, pp. 6757–6764.
- [14] D. Aschenbrenner, C. Colloseus, R. Khoury, and N. Fangerow, “Robot-assisted automated sorting techniques for plastic recycling,” *Procedia CIRP*, vol. 120, pp. 1232–1237, 2023.
- [15] F. Adetunji, A. Karukayil, P. Samant, S. Shabana, F. Varghese, U. Upadhyay, R. Yadav, A. Partridge, E. Pendleton, R. Plant, Y. Petillot, and M. Koskinopoulou, “Vision-based manipulation of transparent plastic bags in industrial setups,” *Frontiers in Robotics and AI*, vol. 12, p. 1506290, 2025.
- [16] M. Leveziel, G. Laurent, W. Haouas, M. Gauthier, and R. Dahmouche, “A 4-dof parallel robot with a built-in gripper for waste sorting,” *IEEE Robotics and Automation Letters*, vol. 7, pp. 9834 – 9841, 10 2022.
- [17] X. Chen, H. Huang, Y. Liu, J. Li, and M. Liu, “Robot for automatic waste sorting on construction sites,” *Automation in Construction*, vol. 141, p. 104387, 09 2022.
- [18] T.-W. Wu, W. Peng, F. Lü, and P.-J. He, “Applications of convolutional neural networks for intelligent waste identification and recycling: A review,” *Resources, Conservation and Recycling*, vol. 190, p. 106813, 03 2023.

- [19] Q. Zhang, Q. Yang, X. Zhang, W. Wei, Q. Bao, J. Su, and X. Liu, “A multi-label waste detection model based on transfer learning,” *Resources, Conservation and Recycling*, vol. 181, p. 106235, 06 2022.
- [20] J. Redmon and A. Angelova, “Real-time grasp detection using convolutional neural networks,” *CoRR*, vol. abs/1412.3128, 2014. [Online]. Available: <http://arxiv.org/abs/1412.3128>
- [21] A. Depierre, E. Dellandréa, and L. Chen, “Jacquard: A large scale dataset for robotic grasp detection,” 03 2018.
- [22] K. S. Marcus Gualtieri, Andreas ten Pas and R. P. Jr, “High precision grasp pose detection in dense clutter,” *CoRR*, vol. abs/1603.01564, 2016. [Online]. Available: <http://arxiv.org/abs/1603.01564>
- [23] A. ten Pas, M. Gualtieri, K. Saenko, and R. Platt, “Grasp pose detection in point clouds,” *International Journal of Robotics Research*, vol. 36, pp. 1455–1473, 12 2017, cross Reference 1.9.
- [24] H. Liang, X. Ma, S. Li, M. Görner, S. Tang, B. Fang, F. Sun, and J. Zhang, “Pointnetgpd: Detecting grasp configurations from point sets,” in *2019 International Conference on Robotics and Automation (ICRA)*, 2019, pp. 3629–3635.
- [25] H.-S. Fang, C. Wang, M. Gou, and C. Lu, “Graspnet-1billion: A large-scale benchmark for general object grasping,” in *2020 IEEE/CVF Conference on Computer Vision and Pattern Recognition (CVPR)*, 2020, pp. 11 441–11 450.
- [26] C. Wang, H.-S. Fang, M. Gou, H. Fang, J. Gao, and C. Lu, “Graspness discovery in clutters for fast and accurate grasp detection,” in *2021 IEEE/CVF International Conference on Computer Vision (ICCV)*, 2021, pp. 15 944–15 953.
- [27] H. Fang, C. Wang, H. Fang, M. Gou, J. Liu, H. Yan, W. Liu, Y. Xie, and C. Lu, “Anygrasp: Robust and efficient grasp perception in spatial and temporal domains,” *IEEE Transactions on Robotics*, vol. 39, pp. 3929–3945, 2022. [Online]. Available: <https://api.semanticscholar.org/CorpusID:254823166>
- [28] J. Mahler, M. Matl, X. Liu, A. Li, D. Gealy, and K. Goldberg, “Dex-net 3.0: Computing robust vacuum suction grasp targets in point clouds using a new analytic model and deep learning,” in *2018 IEEE International Conference on robotics and automation (ICRA)*. IEEE, 2018, pp. 5620–5627.
- [29] C. Correa, J. Mahler, M. Danielczuk, and K. Goldberg, “Robust toppling for vacuum suction grasping,” in *2019 IEEE 15th International Conference on Automation Science and Engineering (CASE)*. IEEE, 2019, pp. 1421–1428.
- [30] H. Cao, H.-S. Fang, W. Liu, and C. Lu, “Suctionnet-1billion: A large-scale benchmark for suction grasping,” *IEEE Robotics and Automation Letters*, vol. 6, no. 4, pp. 8718–8725, 2021.
- [31] A. G. Satav, S. Kubade, C. Amrutkar, G. Arya, and A. Pawar, “A state-of-the-art review on robotics in waste sorting: scope and challenges,” pp. 2789–2806, 12 2023.
- [32] H. T. N. Le and H. Q. T. Ngo, “Application of the vision-based deep learning technique for waste classification using the robotic manipulation system,” *International Journal of Cognitive Computing in Engineering*, vol. 6, pp. 391–400, Dec. 2025.
- [33] W. Xiao, J. Yang, H. Fang, J. Zhuang, Y. Ku, and X. Zhang, “Development of an automatic sorting robot for construction and demolition waste,” *Clean Technol. Environ. Policy*, vol. 22, no. 9, pp. 1829–1841, Nov. 2020.
- [34] L. Chin, J. Lipton, M. C. Yuen, R. Kramer-Bottiglio, and D. Rus, “Automated recycling separation enabled by soft robotic material classification,” *RoboSoft 2019 - 2019 IEEE International Conference on Soft Robotics*, pp. 102–107, 2019, 1.6.

- [35] R. Sadeghian, S. Shahin, and S. Sareh, “Vision-based self-adaptive gripping in a trimodal robotic sorting end-effector,” *IEEE Robotics and Automation Letters*, vol. 7, pp. 2124–2131, 2022.
- [36] X. Wang, B. Wang, J. Pinskiel, Y. Xie, J. Brett, R. Scalzo, and G. Howard, “Fin-bayes: A multi-objective bayesian optimization framework for soft robotic fingers,” *Soft robotics*, vol. 11, 03 2024.
- [37] T. Wu, L. Pan, J. Zhang, T. Wang, Z. Liu, and D. Lin, “Density-aware chamfer distance as a comprehensive metric for point cloud completion,” 2021, arXiv:2111.12702. [Online]. Available: <http://arxiv.org/abs/2111.12702>
- [38] B. G. Greenland, J. Pinskiel, X. Wang, D. Nguyen, G. Shi, T. Bandyopadhyay, J. J. Chung, and D. Howard, “Sograb: A visual method for soft grasping benchmarking and evaluation,” in *2025 IEEE 8th International Conference on Soft Robotics (RoboSoft)*, 2025, pp. 1–6.
- [39] F. Wang and Z. Zhao, “A survey of iterative closest point algorithm,” in *2017 Chinese Automation Congress (CAC)*, 2017, pp. 4395–4399.
- [40] S. Yang, H. Yuan, T. Wang, R. Zhong, C. Song, Y. Fu, W. Ge, and X. Yuan, “Procedural generation of 3d scenes for urban landscape based on remote sensing images,” in *2024 IEEE International Conference on Advanced Video and Signal Based Surveillance (AVSS)*, 2024, pp. 1–7.
- [41] D. W. Hosmer Jr, S. Lemeshow, and R. X. Sturdivant, *Applied logistic regression*. John Wiley & Sons, 2013.
- [42] S. M and P. Sridharan, “Determinants of export diversification: Evidence from fractional logit estimation model,” *Foreign Trade Review*, vol. 57, no. 2, pp. 160–177, 2022.